Colloids and Surfaces A: Physicochemical and Engineering Aspects 702 (2024) 135117

Contents lists available at ScienceDirect

Colloids and Surfaces A: Physicochemical and Engineering Aspects

journal homepage: www.elsevier.com/locate/colsurfa

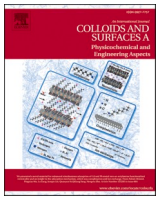

Polyethylene glycol-assisted hydro-solvothermal growth of anisotropic magnetic iron oxides: The role of mixed environment conditions

Gabriele Bona [a], Giulia Bragaggia [b], Matteo Cantoni [c], Barbara Di Credico [a], Silvia Mostoni [a], Giancarlo Capitani [e], Roberto Scotti [a,d], Silvia Gross [b,f,*], Roberto Nisticò [a,**,1]

[a] Department of Materials Science, INSTM, University of Milano-Bicocca, Via R. Cozzi 55, Milano 20125, Italy
[b] Department of Chemical Sciences, University of Padova, Via Marzolo 1, Padova 35131, Italy
[c] Department of Physics, Politecnico di Milano, Via G. Colombo 81, Milano 20133, Italy
[d] Institute for Photonics and Nanotechnologies-CNR, Via alla Cascata 56/C, Povo, (TN), 38123, Italy
[e] Department of Earth and Environmental Sciences, University of Milano-Bicocca, Piazza Della Scienza 1, Milano 20126, Italy
[f] Karlsruher Institut für Technologie (KIT), Institut für Technische Chemie und Polymerchemie (ITCP), Engesserstr. 20, Karlsruhe 76131, Germany

HIGHLIGHTS

- Fe-oxides anisotropic nanoparticles were produced via mixed hydro-solvothermal route.
- Water/PEG and 2-propanol/PEG allow obtaining a predominance of magnetite phase.
- Syntheses performed in mixed environment favor the growth of hematite phase.
- Water/PEG favor nanorod particles, whereas 2-propanol/PEG favor polyhedral systems.
- Samples from water/PEG and 2-propanol/PEG have high magnetic saturation value.

GRAPHICAL ABSTRACT

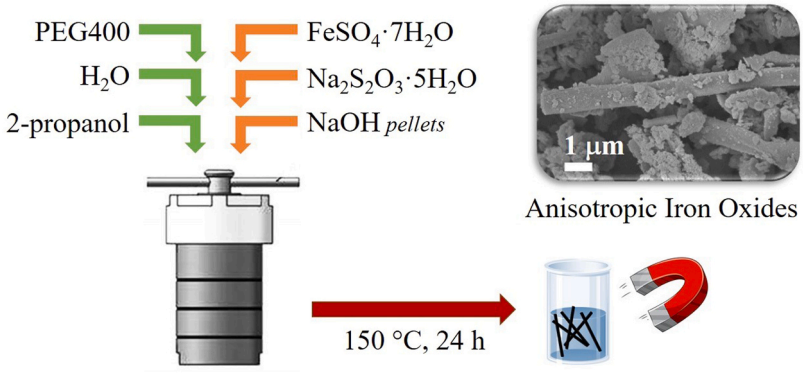

ARTICLE INFO

Keywords:
Colloid chemistry
Hydro-solvothermal synthesis
Iron oxides
Magnetic nanomaterials
Magnetite
Solid state characterization

ABSTRACT

In this study, an alternative mixed hydro-solvothermal route has been investigated for the synthesis of magnetic iron oxide nanoparticles with anisotropic shape. The synthesis was performed at mild conditions (150 °C) in a water/2-propanol environment, using poly(ethylene glycol) (PEG400) as structure directing agent, sodium thiosulfate as reducing agent, and NaOH as precipitating agent. The resulting systems were characterized by combining morphological, structural, and magnetic techniques. Experimental results clearly demonstrate that magnetite/maghemite nanorods are preferentially obtained in water/PEG400 environment, whereas 2-propanol/PEG400 environment promotes the growth of magnetite/maghemite polyhedral systems. Interestingly, synthesis

Abbreviations: 2-pr, 2-propanol; fcc, face-centered cubic; H_c, intrinsic coercivity; M_r, magnetic remanence; M_s, magnetization saturation; NPs, nanoparticles; PEG400, polyethylene glycol with M_n 400; RT, room temperature.

* Corresponding author at: Department of Chemical Sciences, University of Padova, Via Marzolo 1, Padova 35131, Italy.
** Corresponding author.
E-mail addresses: silvia.gross@unipd.it (S. Gross), roberto.nistico@unimib.it (R. Nisticò).
[1] http://orcid.org/0000-0001-8986-5542

https://doi.org/10.1016/j.colsurfa.2024.135117
Received 17 June 2024; Received in revised form 29 July 2024; Accepted 15 August 2024
Available online 21 August 2024

performed in a mixed hydro-solvothermal (*i.e.*, water/2-propanol) environment favors the preferential growth of hematite phase.

1. Introduction

Magnetic nanomaterials have significantly attracted the interest of worldwide scientists due to their wide potential application in a plethora of different advanced technological fields. Among this class of materials, magnetite, which is a mixed ferrous-ferric oxide (Fe_3O_4), deserves a particular interest due to its low-cost, and natural availability, coupled with a quite high magnetic response [1,2]. In particular, bulk magnetite shows an intrinsic ferrimagnetic character due to the presence of unequal antiparallel aligned magnetic moments, whereas when occurring as nanoscopic particles with small dimensions (below *ca*. 20 nm) magnetite shows a superparamagnetic character [3], thus enabling the possibility of exerting a morphologic control a potential powerful approach to further tune its properties [4]. According to the literature, there are numerous studies describing different preparation methodologies for the morphology-controlled synthesis of magnetite nanoparticles (NPs) [5,6]. In this context, soft chemistry strategies (*i.e.*, co-precipitation reactions, micro-emulsion, sol-gel/polyol processes, hydro/solvothermal routes) are extremely powerful techniques for the synthesis of inorganic nanomaterials under mild conditions (below 200 °C), since they are able to pursue also a fine control over the morphology of the final material, even at the nanometer scale [7]. Regarding the hydrothermal and solvothermal routes, both strategies require to the use of solvents as reaction media, water (hydro-) or organic (solvo-), heated above their boiling points in a sealed vessel, with consequent increment of autogeneous pressure, in some cases reaching the supercritical point. Under these conditions, the physical properties of the reaction medium (*e.g.*, viscosity, dielectric constant, boiling point, surface tension, polarity) change significantly, thus allowing a different chemical reactivity (*e.g.*, solubility of precursors), nucleation and growth paths with respect to the ones occurring under normal conditions [8]. A main advantage of both hydro- and solvothermal methods is the possibility of obtaining highly crystalline uncommon metastable nanostructures in a single step [9] already at mild conditions, in many cases without the necessity of performing a second thermal treatment (annealing/calcination), thus saving energy consumption [10]. The choice of the reaction medium in both hydro- and solvothermal routes plays a crucial role in influencing the general properties of the medium (viscosity, dielectric constant, etc.), affecting nucleation and growth phenomena, and acid/base reactivity of the system through hydration/solvation phenomena of the chemical reactive species [11].

Moreover, the properties of the medium influence also the aggregation of the primary particles, with viscosity being inversely proportional to the diffusion coefficient (and, consequently, influencing the mass transfer ability within the medium, according to the Stokes-Einstein relation) [12], and the dielectric constant of the reaction medium affecting the formation of electric charges at the particles surface (and, consequently, influencing the electrostatic stabilization of the colloidal system, according to the Derjaguin-Landau-Verwey-Overbeek, DLVO, theory) [13,14]. In this context, mixtures of solvents allow tuning both viscosity and the dielectric constant of the medium. In fact, as highlighted by He *et al.* [15], different solvents might lead to completely different nanomaterials in terms of composition, crystallinity, polymorphism, morphology (size, shape, and aspect ratio), and surface functionalities. Regarding the use of mixed solvents (rather than a single solvent) in hydro- and solvothermal processes, only few studies have evidenced that this solution can be a very promising route for the synthesis of nanoscopic systems with defined morphology and properties [15]. As demonstrated by Nohara *et al.* [16], water/1,4-butanediol mixed solvent was used as reaction medium for the hydro-solvothermal synthesis of Ce/Tb-doped yttrium borate nanocrystals, showing that the solvent volume ratio influenced the crystallization of the nanomaterials in terms of both primary particles size, and secondary particles size/shape (*i.e.*, evolving from disc-like to polyhedral particles). Moreover, in the study by Miniach *et al.* [17] the hydro-solvothermal synthesis of bismuth sulfide by using water/-ethylene glycol (1:1, v/v) and water/butyldiglycol (1:1, v/v) as reaction medium allowed demonstrating that the mixed environment is beneficial in terms of shape control, with formation of uniform spherical and plate-like particles, respectively. In their study, the authors also reported that the growth of the crystal nuclei is strongly affected by the physical properties of the solvent medium, which influences the diffusion rate of ionic species. More specifically, even iron oxides can be synthesized by using mixed hydro-solvothermal approaches. In particular, Wu *et al.* [18] reported the synthesis of hematite (α-Fe_2O_3) NPs with different shapes obtaining: spherical NPs (from water/cyclohexanol environment, and ammonia as precipitating agent), rod-like systems (from water/cyclohexanol environment, and sodium hydroxide as precipitating agent), and disk-like morphologies (from pure cyclohexanol environment, and ammonia as precipitating agent). However, the authors provided no considerations regarding the growth mechanism. Interestingly, Zhang *et al.* [19] reported the synthesis of magnetite NPs from a mixed water/ethylene glycol environment following a mixed hydro-solvothermal route. As highlighted by the authors, the solvent volume ratio played an important role in controlling the morphology (in terms of size, shape, porosity) of the resulting magnetite NPs, with large non-porous spherical particles obtained using ethylene glycol as solvent (*i.e.,* pure solvothermal condition), and a progressively decrease of the spherical particles average size by gradually increasing the water content with formation of mesopores. Remarkably, in the case of bare water environment (*i.e.*, pure hydrothermal condition) large non-porous polyhedral hematite (α-Fe_2O_3) NPs were obtained. The authors rationalized the results pointing out the twofold role played by both solvents, with ethylene glycol acting as solvent and reducing agent, and water acting as solvent and binder able to coordinate ferric ions. Nevertheless, water played also a fundamental role in controlling the solubility of urea, and consequently the release of the precipitating agent hydroxide ions (OH^-). Lastly, Xin *et al.* [20] exploited a mixed hydro-solvothermal approach (using water/ethanol as reaction medium and ammonia as precipitant) to grow a titania (anatase phase) shell over the magnetite spherical NPs.

In general, the analysis of the state-of-the-art literature reveals that all the retrieved case studies based on mixed hydro-solvothermal routes, evidenced the role played by the reaction medium (and the solvent composition) in influencing the final morphology of the systems, but no direct correlations were unveiled.

Hence, the present study aims at investigating the synthesis of anisotropic magnetite NPs following a mixed hydro-solvothermal route performed at mild conditions (150 °C), using a water-2-propanol (2-pr.) mixture as reaction medium, in presence of poly(ethylene glycol) (PEG400) as structure directing agent, sodium thiosulfate as reducing agent, and NaOH as precipitating agent. The effects of the process parameters over the final morphology were in depth analyzed, focusing on the role of the compositional parameters (*i.e.*, primarily the solvents volume ratio) in defining the final morphology and chemical composition of the resulting nanomaterials. A systematic variation of the different experimental parameters was performed to explore the possibility to tune the final features of the materials. Morphological, and structural features of the iron oxides produced with the mixed hydro-solvothermal route were monitored by means of scanning electron microscopy (SEM), X-ray powder diffraction (XRD), and the most representative samples by means of transmission electron microscopy (TEM)

to confirm the final structure, and vibrating sample magnetometry (VSM) to monitor the magnetic response. Lastly, the possible relationships between the experimental/compositional parameters of the reaction medium and the morphology and chemical composition of the resulting nanomaterials were provided. To the best of the authors knowledge, this is the first time that a mixed hydro-solvothermal approach, using a complex water/2-propanol reaction medium in the presence of PEG400, has been used to directly synthesize anisotropic magnetic iron oxide NPs.

With respect to the majority of the state-of-the-art literature on systems obtained from mixed hydro-solvothermal routes, in the present study authors have tried to provide correlations between the final morphology and chemical structure of the iron oxides with the different environment conditions, trying to find a rationale.

2. Experimental section

2.1. Chemicals

Chemicals: Iron(II) sulphate heptahydrate ($FeSO_4{\cdot}7\ H_2O$, ACS reagent, 98 %, CAS 7782–63–0, Thermo Scientific), sodium thiosulfate pentahydrate ($Na_2S_2O_3{\cdot}5\ H_2O$, ACS reagent, ≥ 99.5 %, CAS 10102–17–7, Sigma Aldrich), and sodium hydroxide pellets (NaOH, puriss., p.a., ACS reagent, ≥ 98 %, CAS 1310–73–2, Sigma Aldrich) were used as received.

Solutions and solvents: 2-propanol (C_3H_8O, 2-pr., anhydrous, 99.5 %, CAS 67–63–0, Sigma-Aldrich), poly(ethylene glycol) (PEG400, $H(OCH_2CH_2)_nOH$, M_n 400, CAS 255322–68–3, Sigma-Aldrich), acetone (CH_3COCH_3, CAS 67–64–1, Sigma-Aldrich). Furthermore, deionized water is used during washing procedures. Milli-Q water with a resistivity of 18.2 MΩ cm was used. All chemicals were used without further purification.

2.2. Hydro-solvothermal synthesis of anisotropic magnetite

Magnetic iron oxides were prepared following a properly modified procedure taken from the literature [21]. In a typical synthesis, $FeSO_4{\cdot}7\ H_2O$ (depending on the synthesis the following quantity were investigated, namely: either 1.112 g, or 2.2240 g) and $Na_2S_2O_3{\cdot}5\ H_2O$ (either 0.4963 g, or 0.9926 g) were manually mixed/ground by means of an agate mortar, and transferred into a 23 mL A255AC Teflon-lined stainless hydrothermal reactor (*Parr Instrument Company, Illinois, USA*). Subsequently, solvents with variable compositions were preliminary mixed and introduced into the autoclave, to get a filling ratio of 40 % (thus considering a final volume of 10 mL). The solvents were PEG400 (which acts both as stabilizer and structure directing agent), water, and 2-propanol ("2-pr." in the following). Different volume ratios between solvents were investigated, namely: (i) water/PEG400 100/0, 75/25, 50/50, 25/75, v/v; (ii) 2-pr./PEG400 100/0, 75/25, 50/50, 25/75, v/v; (iii) water/2-pr./PEG400 37.5/12.5/50, 25/25/50, 12.5/37.5/50, v/v. The different compositional parameters and solvents ratios are reported in Table 1. A constant amount of NaOH pellets (2 g, 50 mmol) was added directly into the autoclave. Afterwards, the mixture was thermally treated in a pre-heated oven at 150 °C for 24 h. Subsequently, the autoclave was allowed to naturally cool down to room temperature (RT). Suspensions were centrifuged at 12,000 revolutions per minute (rpm) for 3 min., washing with deionized water (three times) and acetone (one time). Samples were oven dried under air atmosphere at 70 °C overnight. Lastly, dried nanomaterials were gently crumbled inside an agate mortar, and samples storage inside closed glass vials. A typical yield of this chemical route is *ca*. 96 %. The obtained samples were labeled as S-NN (acronym of Sample-NN, with NN being a progressive number corresponding to the experimental conditions reported in Table 1). A schematic representation of the general PEG-assisted hydro-solvothermal route here investigated is reported in Fig. 1.

Table 1
Samples synthesized and used compositional parameters.

Sample	$FeSO_4{\cdot}7\ H_2O$: $Na_2S_2O_3{\cdot}5\ H_2O$ molar ratio	H_2O: 2-pr.: PEG400 volume ratio
S−01	2	1.000: 0.000: 0.000
S−02	2	0.750: 0.000: 0.250
S−03	2	0.500: 0.000: 0.500
S−04	2	0.250: 0.000: 0.750
S−05	2	0.000: 1.000: 0.000
S−06	2	0.000: 0.750: 0.250
S−07	2	0.000: 0.500: 0.500
S−08	2	0.000: 0.250: 0.750
S−09	2	0.375: 0.125: 0.500
S−10	2	0.250: 0.250: 0.500
S−11	2	0.125: 0.375: 0.500
S−12	1	0.500: 0.000: 0.500
S−13	1	0.000: 0.500: 0.500
S−14	1	0.250: 0.250: 0.500
S−15	4	0.500: 0.000: 0.500
S−16	4	0.000: 0.500: 0.500
S−17	4	0.250: 0.250: 0.500

2.3. Characterizations

SEM micrographs were collected by means of a Zeiss Gemini 500 microscope equipped with a traditional secondary electrons' detector. Samples were deposited onto SEM stubs using a double-adhesive carbon tape and covered with a gold coating to avoid any charging effect using an Edwards S150B sputter coater.

Transmission electron microscopy (TEM) images and selected areas electron diffraction (SAED) patterns were collected by means of a JEOL JEM-2100Plus (Jeol, Japan) instrument. The TEM operated with an acceleration voltage of 200 kV, and equipped with a 9-megapixel Gatan (Gatan, USA) Rio Complementary Metal-Oxide-Superconductur (CMOS) camera. Samples were deposited onto carbon coated Cu TEM mesh grids by drop-casting a dilute dispersion of the nanomaterials in ethanol.

XRD patterns were recorded by means of a Rigaku Miniflex 600, working with a Cu source (40 kV, 15 mA), scanning in the 20–70°2θ range, step size of 0.02 degrees, angular velocity 5.0 degrees per minute. Instrumental PDXL-2 software was used for comparison with reference diffraction patterns from the ICDD database.

Magnetization curves were recorded by means of an EZ-9 MicroSense Magnetometer VSM, with resolution of 1 μemu and maximum field of 2.25 T. Measurements were performed at RT, using quartz cuvettes as sample holder (the diamagnetic contribution due to empty cuvettes was automatically subtracted). The absence of any ferromagnetic spurious contribution from the cuvettes was verified before any measurement.

3. Results and discussion

To facilitate the readability and remark the most important findings, this section has been organized into three main sections. *Paragraph 3.1* reports the morphological (SEM and TEM, the latter one only on two selected samples) and structural (XRD) characterizations of all the samples prepared, whereas *Paragraph 3.2* reports the magnetic (VSM) characterization (only on four selected samples). The main relevant findings (with depicted trends) and the possible explanations of how the different parameters have influenced the final morphology and chemical composition of the different samples is reported in a dedicated section (*Paragraph 3.3*).

3.1. Morphological and structural characterizations

The effect of the different mixed solvents compositions on the morphology of the resulting nanomaterials was investigated by means of SEM analysis (high magnification SEM micrographs of all samples are reported in the Supporting Information section). The morphological characterization of samples obtained using either water/PEG400 or 2-

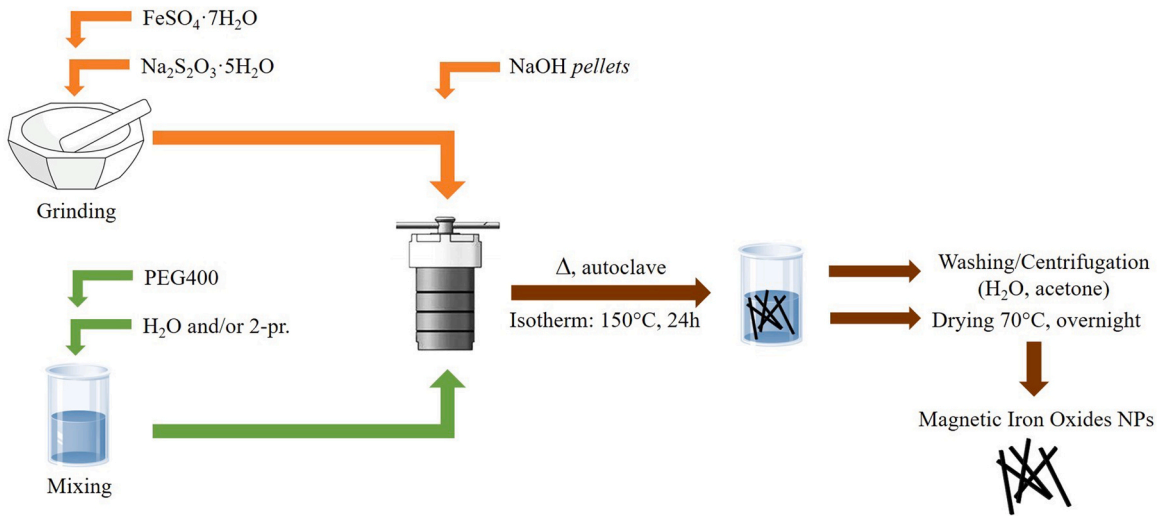

Fig. 1. Schematic representation reporting the hydro-solvothermal route for the direct synthesis of the magnetic iron oxides.

pr./PEG400 mixtures as reaction medium, varying the solvents/PEG400 volume ratio, are reported in Fig. 2. SEM image of S-01 sample obtained from a bare hydrothermal environment (in absence of PEG400) highlights the occurrence of a prevailing polyhedral morphology with particles presenting an average diameter in the 500–750 nm range (Fig. 2A). By gradually introducing PEG400, the formation of prevailing anisotropic morphologies constituted by thin nanorods is appreciable (samples S-02, S-03, and S-04, Fig. 2B, Fig. 2C, Fig. 2D, respectively). In particular, by increasing the volume of PEG400 the co-presence of lamellar systems of large dimensions was observed. According to this trend, S-02 (Fig. 2B), with the highest water/PEG400 ratio, seems to be the most homogeneous one (*i.e.*, in terms of prevailing morphology), with nanorods of *ca.* 1 μm length, and *ca.* 100 nm thickness (and a consequent aspect ratio, AR, of *ca.* 10). The formation of anisotropic NPs can be speculated considering the PEG molecules coordination ability and assemblage in aqueous environment [22,23]. In particular, Chen *et al.* [23] reported that Fe ions and PEG molecules form a relatively stable complex. In presence of hydroxide ions (deriving from the alkaline environment), it is expected a gradual replacement of the PEG molecules in the coordination respect to Fe ions (*i.e.*, coordination bond strength with metal ions: $HO^- >$ PEG). Furthermore, as reported by Wang *et al.* [22], once dissolved in water environment non-ionized surfactants (such as PEG molecules) are able to self-assemble into chain-like supramolecular structures, thus forming one-dimensional liquid confined spaces where nanoclusters are forced to grow linearly, along a preferential spatial direction, inhibiting the agglomeration phenomena, thus favoring the formation of nanorods in such confined environment. Interestingly, PEG molecules continuously adsorb at the surface of formed nuclei with different adsorption strength on the different crystal faces, causing the faster growth of nanocrystals in the direction with lower surfactant adsorption.

Regarding the sample S-05 obtained from a bare 2-pr. solvothermal environment, instead, a prevailing polyhedral morphology occurs with very large particles presenting average diameters in the *ca.* 1.5–3.0 μm range (Fig. 2E). Interestingly, the addition of PEG400 to 2-pr. solvent caused a retain of a prevailing polyhedral morphology, with S-06 (Fig. 2F) being the most homogeneous sample obtained from the 2-pr./PEG400 mixture; however, in this case, the particles are remarkably smaller than those obtained in absence of PEG400 (with diameters of *ca.* 230 nm). Even in this case, an increment of the morphologic disorder by increasing PEG400 was pointed out, with a prevalence of polyhedral morphologies, but in co-presence with important lamellar structures, as in S-07 (Fig. 2G), and S-08 (Fig. 2H).

XRD analysis in Fig. 3 was performed to investigate the formation of specific crystalline structures. The XRD patterns of S-01, S-02, S-03 and S-04 samples obtained using water/PEG400 (Fig. 3A) show the presence

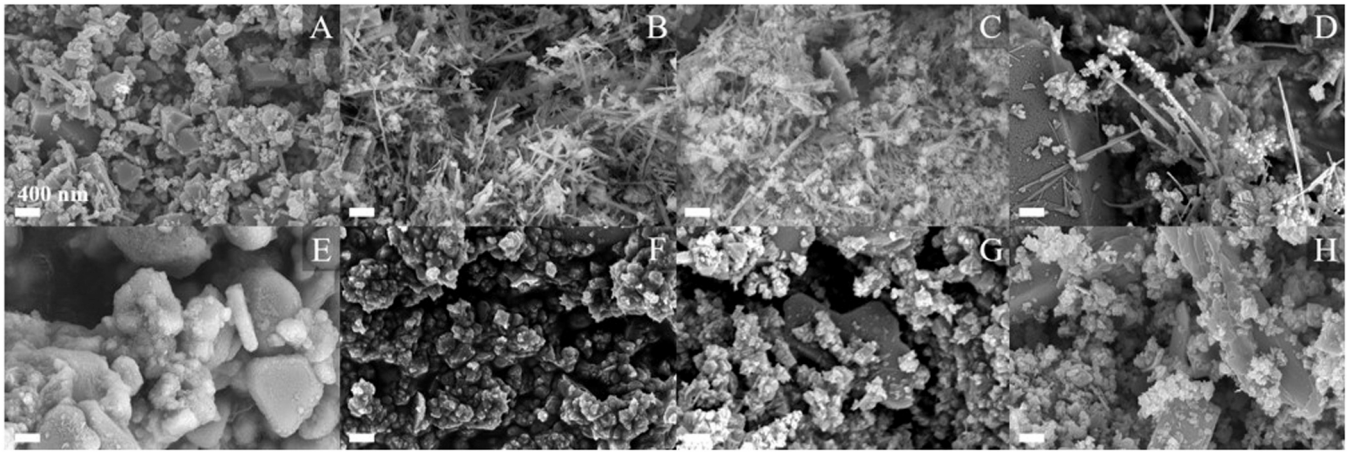

Fig. 2. SEM micrographs of samples obtained in water/PEG400 environment (top), and 2-pr./PEG400 environment (bottom), at increasing PEG400 content, from 100/0 (A, E), 75/25 (B, F), 50/50 (C, G), 25/75 (D, H), from left to right respectively. Legend: S-01 (A), S-02 (B), S-03 (C), S-04 (D), S-05 (E), S-06 (F), S-07 (G), and S-08 (H). All micrographs were collected at the same magnification.

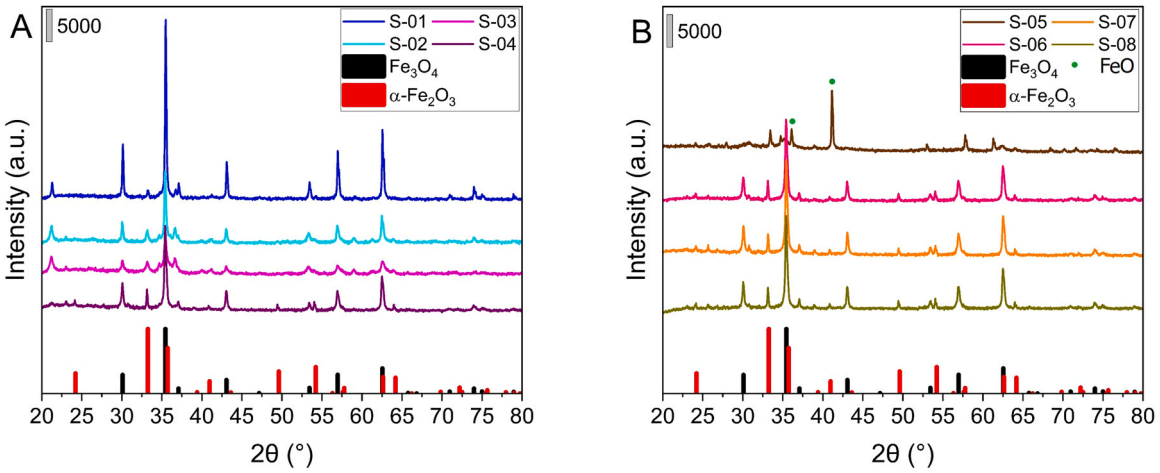

Fig. 3. XRD patterns of samples obtained in water/PEG400 environment (A, left), and 2-pr./PEG400 environment (B, right), varying the solvents/PEG400 ratio. Panel (A): S-01 (100/0, blue), S-02 (75/25, cyan), S-03 (50/50, magenta), S-04 (25/75, purple). Panel (B): S-05 (100/0, brown), S-06 (75/25, pink), S-07 (50/50, orange), and S-08 (25/75, dark yellow). XRD reference patterns: magnetite (01–074–0748, Fe_3O_4, black), and hematite (01–089–8104, α-Fe_2O_3, red). *Note*: Signals in sample S-05 attributed to the presence of wustite (00–006–0696, FeO) are marked with green dots.

of the main crystal reflection planes at 2θ = 30.1° (220), 35.4° (311), 43.1° (400), 53.4° (422), 57.0° (333), and 62.6° (440), associated to magnetite (PDF 01–074–0748, ICDD) [24]. However, the possible presence of maghemite phase (γ-Fe_2O_3) cannot be totally excluded since magnetite and maghemite cannot be distinguished by XRD characterization, and it is well known that magnetite can easily evolve into maghemite through topotactic oxidation [24,25]. Furthermore, traces of other iron oxide phases were registered, mainly attributable to hematite α-Fe_2O_3 (PDF 01–089–8104, ICDD) at 2θ = 24.1° (012), 33.2° (104), 35.6° (110), 40.8° (113), 49.4° (024), 54.0° (116), 62.4° (214), and 63.9° (300) [26]. In particular, the intensity of the magnetite reflections seems decreasing with the water/PEG400 volume ratio (with the highest crystallinity in the case of S-01), whereas hematite signals become more relevant by increasing the PEG400 content, particularly in S-04. The magnetite-to-hematite phase transition is a well-documented phenomenon occurring principally following a redox-independent reaction, even if an oxidant excess speeds up the kinetics of this transformation. According to Zhao *et al.* [27], the replacement of magnetite into hematite is primarily driven by the leaching of ferrous ions from magnetite. This latter phenomenon is kinetically driven by the variation of temperature and solution parameters (*i.e.*, pH and concentrations of ligands), all factors influencing the transport of both ferrous ions and oxidant to the reaction front. Additionally, Li *et al.* [28], investigated the stability of magnetite under oxidizing alkaline hydrothermal conditions (*i.e.*, in presence of dissolved oxygen). Authors registered that the oxidation kinetics is consistent with a diffusion-controlled process involving the release of ferrous ions from magnetite, and the subsequently oxidation to aqueous ferric hydroxide ($Fe(OH)_3$), which reprecipitates forming hematite. Therefore, a possible explanation of the curious trend registered in our systems could be attributed to a higher difficulty of both the reducing agent (*i.e.*, thiosulfate ions) and the precipitating agent (*i.e.*, hydroxide ions) to effectively reach the iron ions in presence of high content of PEG400 molecules, which self-assembled when mixed in aqueous environment forming chain-like supramolecular structures. However, this is just a speculation, which would require an in-depth analysis. Interestingly, despite the presence of traces of the antiferromagnetic hematite, it has been verified that all samples are magnet-sensitive by applying an external magnetic field in presence of a neodymium magnet.

Even in the case of 2-pr./PEG400 systems (S-05, S-06, S-07, and S-08, Fig. 3B), analogous results to water/PEG400 series were reached, with the main relevant signals attributable to magnetite phase, and the co-presence of traces of hematite. The only exception seems sample S-05 (obtained in a bare 2-pr. reaction environment), which shows an XRD pattern not directly ascribable to magnetite/maghemite, but the presence of both: (i) the crystal reflection planes at 36.1° and 42.1° attributable to traces of wustite (FeO) phase (PDF 00–006–0696, ICDD) [29,30], which is a metastable iron oxide phase [31], and (ii) the crystal reflection plane at 33.2° attributable to the possible presence of traces of hematite. The TEM-SAED analysis performed on both samples S-02 and S-06 confirmed the output from the SEM analysis. In particular, the TEM analysis revealed in the case of sample S-02 the formation of nanorods, whereas regarding sample S-06 the analysis revealed the presence of polyhedral nanoparticles, whose average in-plane size is estimated being *ca.* 200 nm. Finally, the SAED analysis performed for both samples releveled the presence of some of the main relevant signals attributable to magnetite phase, in particular the signals at d_{hkl} *ca.* 2.5 Å (311), *ca.* 1.8 Å (420), and *ca.* 1.5 Å (440) (for details please consider the dedicated Supporting Information section).

Fig. 4 shows the morphological characterization of samples obtained from a mixed water/2-pr./PEG400 reaction medium. Generally, this class of samples shows a less defined morphology, and a general lower degree of anisotropy. The only exception is the sample S-10 (Fig. 4B), which shows the presence of both lamellar systems of *ca.* 2 μm size, and thick nanorods whose dimensions are *ca.* 6–8 μm length and *ca.* 300 nm thickness (AR equal to 0.5). These nanorods are remarkably thicker with respect to those obtained from water/PEG400 reaction medium.

Concerning the XRD measurements (Fig. 5), the strongly predominant presence of the characteristic signals of hematite phase rather than magnetite is evident, especially in the samples S-09 and S-10, which in fact are non-magnetic. On the contrary, the composition of the magnetic sample S-11 is not directly assignable to a well-defined single crystal phase, even if it is possible to appreciate the presence of a crystal reflection at 35.5°, which is characteristic of the magnetite/maghemite and hematite phases.

By doubling the amount of sodium thiosulfate in water/PEG400 environment, a decrease of the nanorods fraction can be appreciated (S-03, Fig. 6A) in favor of a predominance of lamellar systems (S-12, Fig. 6D). Interestingly, samples S-10 and S-14 obtained in mixed water/2-pr./PEG400 reaction medium are characterized by the predominant formation of nanorods with an increased homogeneity in the case of S-14 (Fig. 6E), whose dimensions are *ca.* 6 μm length, and *ca.* 1 μm thickness (AR equal to 0.17). Analogously to water/PEG400, even the sample obtained in a 2-pr./PEG400 shows a retainment of the morphology of sample S-07 (S-13, Fig. 6F).

XRD analyses in Fig. 7 reported a predominance of the characteristic

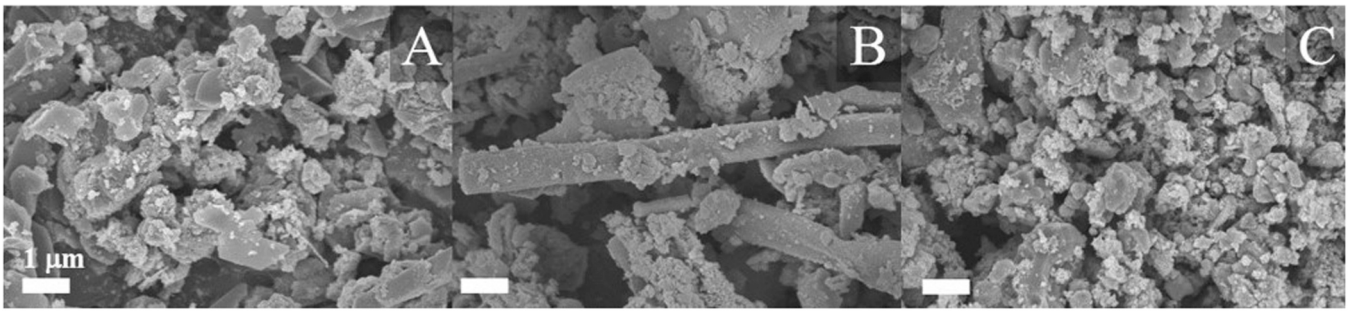

Fig. 4. SEM micrographs of samples obtained in mixed solvents/PEG400 50/50 environment, maintaining constant the volume of PEG400, and varying the water/2-pr. ratio, namely: S-09 (75/25, A, left), S-10 (50/50, B, middle), and S-11 (25/75, C, right). All micrographs were collected at the same magnification.

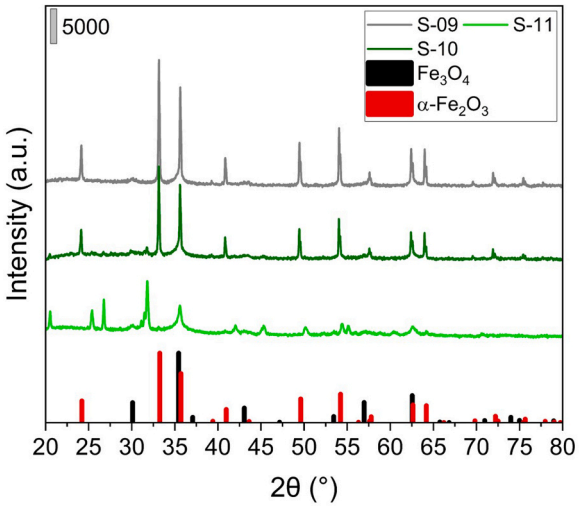

Fig. 5. XRD patterns of samples obtained in mixed solvents/PEG400 50/50 environment, maintaining constant the volume of PEG400, and varying the water/2-pr. ratio, namely: S-09 (75/25, grey), S-10 (50/50, olive), and S-11 (25/75, green). XRD reference patterns: magnetite (01–074–0748, Fe_3O_4, black), and hematite (01–089–8104, α-Fe_2O_3, red).

signals due to hematite phase rather than the magnetite, especially in sample S-12. This result is quite interesting, especially if compared to the analogous sample S-03 obtained at half amount of sodium thiosulfate, primarily made of magnetite phase (see Fig. 3A). On the contrary, both samples S-13 and S-14 display the characteristic signals of magnetite and hematite, together with different extra peaks not directly assignable to a specific crystal phase. In particular, sample S-10 is primarily made by hematite phase (see Fig. 5), whereas S-07 is primarily made by magnetite phase together with traces of hematite phase (see Fig. 3B). The evaluation in presence of a commercial neodymium magnet confirms that sample S-12 is not sensible to the magnet since largely made by hematite phase, which is primarily antiferromagnetic (with very low spontaneous magnetization) [32].

By doubling the content of the precursor iron sulphate, the morphological characterization in Fig. 8 highlights an increment of nanorods size in sample S-15 obtained in water/PEG400 environment, whose dimensions are *ca.* 9 µm length, and *ca.* 600 nm in thickness (AR = 0.07, Fig. 8D). Regarding the sample S-17 obtained in mixed hydro-solvothermal conditions (Fig. 8E), it is possible to appreciate an increment of nanorods as predominant morphology. Peculiarly, in the case of sample S-16 obtained in 2-pr./PEG400 environment the highest iron concentration caused a change in the final morphology, with the formation of a homogeneous system constituted by polyhedral NPs with dimensions in the 300–700 nm range (Fig. 8F).

XRD diffractograms of both samples S-15 and S-17 (Fig. 9A) reveal the main characteristic signals due to both magnetite and hematite phases (with a prevalence of hematite in the case of S-17), whereas sample S-16 (Fig. 9B) shows signals at 2θ = 28.5° (111), 33.0° (200), 37.1° (210), 40.8° (211), 47.4° (220), 56.3° (311), 59.0° (222), 61.7° (023), 64.3° (321), 76.6° (331), and 79.0° (420), which can be associated to the presence of pyrite (FeS_2) phase (PDF 01–071–2219, ICDD) [33,34]. In particular, this very peculiar result is partially in agreement with the study written by E'jazi *et al.* [35], where it has been demonstrated that FeS_2 phase is obtained when using $FeSO_4$ and $Na_2S_2O_3$ with molar ratio 1:4 in solvothermal conditions (using ethanol as solvent) at temperature below 200 °C, with $Na_2S_2O_3$ acting also as a source of S.

3.2. Magnetic characterizations

According to the literature [36], the occurrence of magnetic response in nanomaterials is not only due to their chemical composition, but other relevant factors are important, such as: the particle size, shape, and self-assembling. In order to investigate the magnetic performances of the nanosystems synthesized following the hydro-solvothermal approaches here proposed, four representative samples were selected, namely: S-02 (*i.e.*, magnetite nanorods with AR 10 with traces of hematite obtained from water/PEG400 75/25), S-06 (*i.e.*, magnetite polyhedral systems with traces of hematite obtained from 2-pr./PEG400 75/25), S-10 (*i.e.*, hematite lamellar systems with magnetite nanorods with AR 0.5 obtained from water/2.pr./PEG400 25/25/50 at low content of $Na_2S_2O_3{\cdot}5\ H_2O$) and S-14 (*i.e.*, hematite lamellar systems with magnetite nanorods with AR 0.17 obtained from water/2.pr./PEG400 25/25/50 at high content of $Na_2S_2O_3{\cdot}5\ H_2O$). These samples were selected among the others for the following reasons, namely:

- S-02 is the most homogeneous sample showing a nanorod prevailing morphology, whereas S-06 shows a prevailing polyhedral morphology. Both samples contain both magnetite/maghemite and hematite phases;
- S-10 shows a nanorod prevailing morphology, but it is primarily made by hematite phase;
- S-14 is the analogous of S-10, obtained at higher content of sodium thiosulfate.

The magnetic properties of the selected samples were evaluated by means of magnetization curves measured at RT by means of VSM as reported in Fig. 10 (numerical values are summarized in Table 2).

According to the acquired experimental data, S-02 sample is primarily superparamagnetic, showing a magnetization saturation (M_s) value of *ca.* 41 emu g^{-1}, with a narrow hysteresis loop with magnetic remanence (M_r) of *ca.* 3 emu g^{-1} and intrinsic coercivity (H_c) of *ca.* 46.5 Oe. S-06 is very similar to S-02, showing M_s of *ca.* 52 emu g^{-1}, M_r of *ca.* 8 emu g^{-1}, and a larger hysteresis, having H_c of *ca.* 132 Oe. In the case of samples S-10 and S-14 (both primarily made by hematite phase), it is registered a drop of the M_s values (*i.e.*, below 14 emu g^{-1}) and an almost negligible hysteresis loop with M_r below 1 emu g^{-1} and H_c below

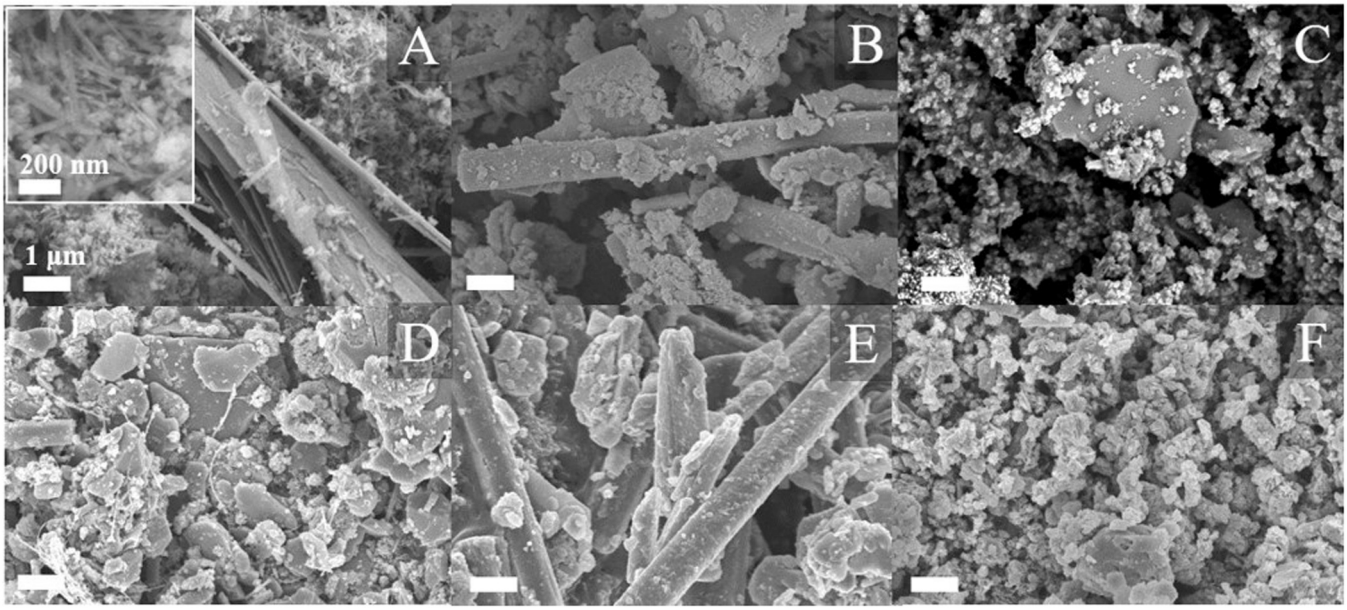

Fig. 6. SEM micrographs of samples obtained in water/PEG400 50/50 environment (A, D, left), mixed solvents/PEG400 50/50 environment with water/2-pr. 50/50 ratio (B, E, middle), and 2-pr./PEG400 50/50 environment (C, F, right), varying the amount of $Na_2S_2O_3{\cdot}5\ H_2O$ from 0.4963 g (2 mmol, top), to 0.9926 g (4 mmol, bottom), namely: S-03 (A), S-10 (B), S-07 (C), S-12 (D), S-14 (E), S-13 (F). All micrographs were collected at the same magnification. Inset in Panel A refers to the relative sample (i.e., S-01) at high magnification.

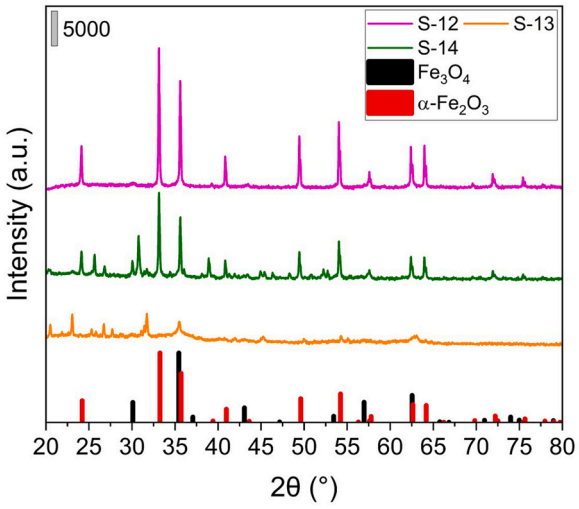

Fig. 7. XRD patterns of samples obtained in water/PEG400 50/50 environment, mixed solvents/PEG400 50/50 environment with water/2-pr. 50/50 ratio, and 2-pr./PEG400 50/50 environment, at high content of $Na_2S_2O_3{\cdot}5\ H_2O$ (*i.e.*, 0.9926 g, 4 mmol), namely: S-12 (magenta), S-14 (olive), S-13 (orange). XRD reference patterns: magnetite (01–074–0748, Fe_3O_4, black), and hematite (01–089–8104, α-Fe_2O_3, red).

30 Oe. Interestingly, sample S-02 profile is much more complex than the others, as it seems that at H-values near zero S-02 follows the behavior of the previously described S-10 and S-14 samples (namely, a narrowing of the hysteresis loop), whereas at high value of magnetic field, S-02 seems more similar to S-06. This very particular trend could be rationalized considering that the chemical composition of these systems is a mixture of magnetite and hematite phases with only the former one effectively being magnet-sensitive. Thus, their magnetic performance is primarily influenced by the amount of magnetite phase, and only at a second level influenced by the NPs shape. However, by keeping this in mind, it seems that the S-02 and S-06 samples are comparable between each other due to their chemical composition with high content of magnetite (and probably higher in the case of S-06 respect to S-02). Analogously, both S-10 and S-14 are comparable between each other, even here the chemical composition plays a major role, in agreement with the XRD characterization, since primarily made by the poorly magnetic phase hematite. However, regarding the effect of the morphology on the magnetic performance of these systems, the M_s of NPs with a given composition is directly regulated by their size [37], even if there are studies highlighting that 4 nm size showed M_s values almost equal to their bulk counterparts [38]. This behavior clearly demonstrates that a direct correlation between NPs size and magnetic response is not a trivial point. Anyway, as clearly highlighted by Lu *et al.* [39], the magnetic response of NPs is affected by both bulk size effects and surface effects. Among the bulk size effects, there are the single-domain (superparamagnetic) limit (which depends on the material chemical composition), the size effect (*i.e.*, small NPs have high coercivity), and the shape effect (*i.e.*, high aspect ratio induce high coercivity). Furthermore, among the surface effects there is the presence of a magnetically inert coating at the NPs surface. Therefore, trying to make a correlation also with the NPs morphology, it seems that the small polyhedral morphology of sample S-06 seems favoring an increment of the hysteresis loop (with an increase of both M_r and H_c), compared to the magnetization curve profile of sample S-02, primarily made by long nanorods (with AR 10).

3.3. Considerations over the synthesis conditions

As reported in the previous section, the experimental efforts were aimed to a systematic exploration of one part of experimental parameters space, involving variation in precursors molar ratios, composition and volume ratios in the solvent mixtures to pinpoint the role of both on the structural and morphological evolution of the resulting oxides. Due to the large number of synthesized samples and investigated parameters, to find a rationale to the synthesis approach here proposed, ternary diagrams are plotted in Fig. 11, and output reported in Table 3. Apart from few exceptions, results clearly indicate what follows:

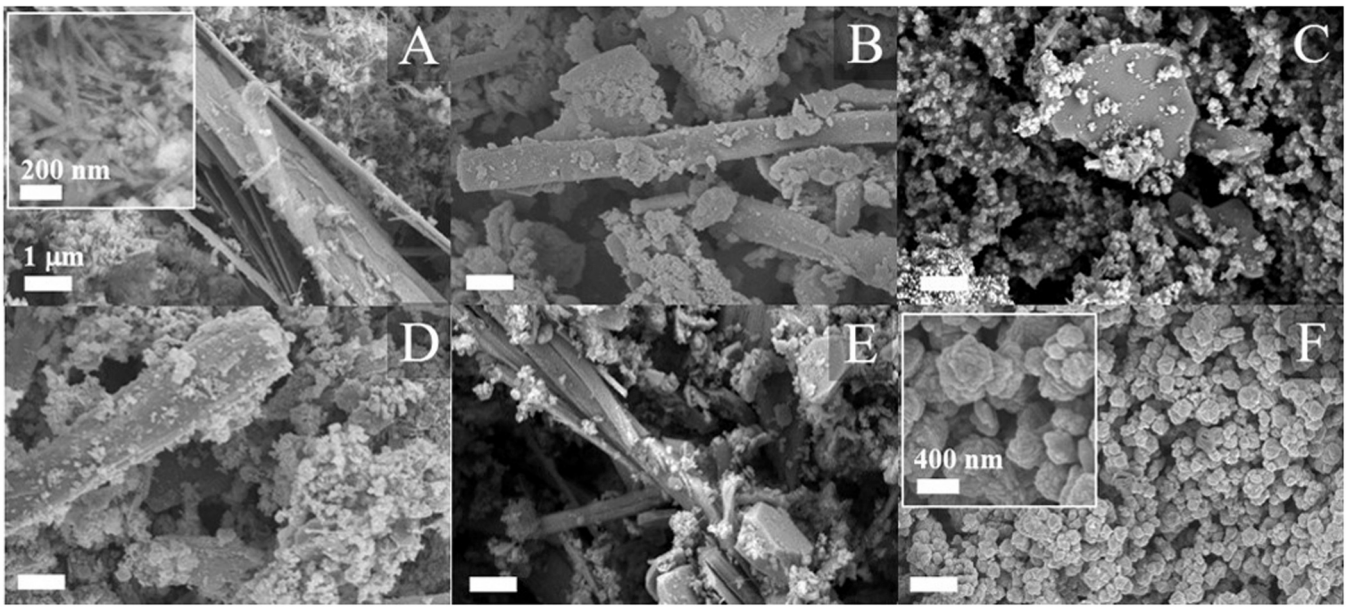

Fig. 8. SEM micrographs of samples obtained in water/PEG400 50/50 environment (A, D, left), mixed solvents/PEG400 50/50 environment with water/2-pr. 50/50 ratio (B, E, middle), and 2-pr./PEG400 50/50 environment (C, F, right), varying the amount of $FeSO_4{\cdot}7\ H_2O$ from 1.112 g (4 mmol, top), to 2.224 g (8 mmol, bottom), namely: S-03 (A), S-10 (B), S-07 (C), S-15 (D), S-17 (E), S-16 (F). All micrographs are collected at the same magnification. Insets in Panels A and F refer to the relative samples (i.e., S-01 and S-16, respectively) at high magnification.

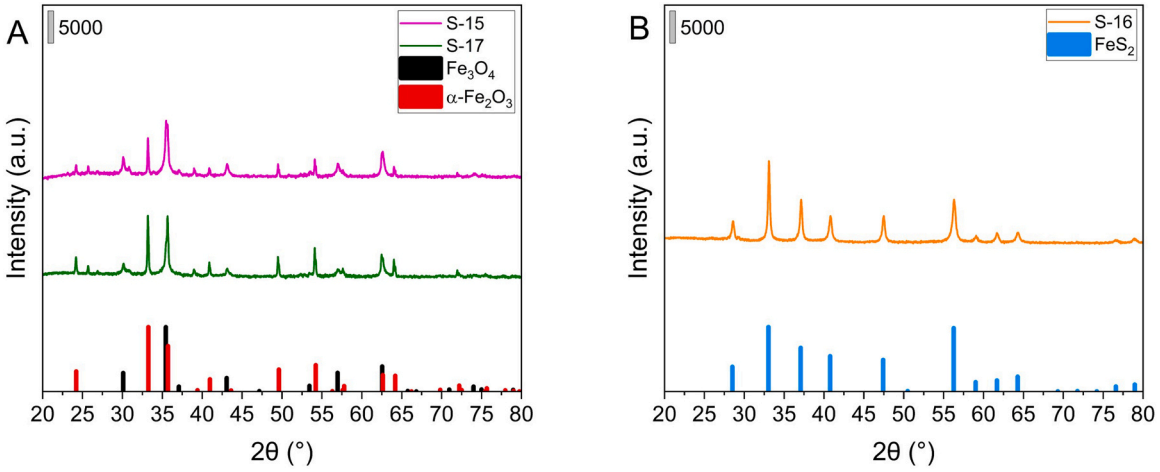

Fig. 9. XRD patterns of samples obtained in water/PEG400 50/50 environment (A, left), mixed solvents/PEG400 50/50 environment with water/2-pr. 50/50 ratio (A, left), and 2-pr./PEG400 50/50 environment (B, right), at high content of $FeSO_4{\cdot}7\ H_2O$ (*i.e.*, 2.224 g, 8 mmol). Panel (A): S-15 (magenta), and S-17 (olive). Panel (B): S-16 (orange). XRD reference patterns: magnetite (01–074–0748, Fe_3O_4, black), hematite (01–089–8104, α-Fe_2O_3, red), pyrite (01–071–2219, FeS_2, blue).

1) Synthesis performed in either water/PEG400 or 2-pr./PEG400 allows obtaining nanomaterials with a clear predominance of magnetite/maghemite phase with traces of hematite phase.
2) Synthesis performed in mixed water/2-pr./PEG400 favors the growth of hematite phase over the other phases.
3) Increasing the amount of sodium thiosulfate seems favoring the formation of magnetite/maghemite phase with respect to the hematite phase.
4) Synthesis performed in water/PEG400 allows obtaining particles with a prevalence of nanorods together with lamellar systems.
5) The presence of PEG400 is mandatory (but not sufficient) for the formation of nanorod particles as prevalent shape (*i.e.,* synthesis performed on a simple water environment in absence of PEG400 allows obtaining a predominance of polyhedral morphology).
6) Synthesis performed in 2-pr./PEG400 allows obtaining particles with prevalence of polyhedral morphology.
7) Synthesis performed in mixed water/2-pr./PEG400 produces polyhedral particles; the only exception seems the sample with equal amount of water/2-pr., which evolved toward a mixed nanorods and lamellar systems.
8) In the case of the synthesis performed in mixed water/2-pr./PEG400 with equal amount of water/2-pr., nanorods obtained are much thicker than in the case of their analogous obtained in a water/PEG400 environment (*i.e.*, in absence of 2-pr.).

Therefore, based on these results, anisotropic iron oxides with magnetic features can be obtained performing the synthesis primarily in hydrothermal conditions (*i.e.,* water/PEG400 environment), eventually at high content of reducing agents (*i.e.*, sodium thiosulfate).

According to the literature, PEG plays a fundamental twofold role in favoring the growth of anisotropic systems [40,41,56] due to its ability to form both a stable complex with Fe ions, gradually replaced by the

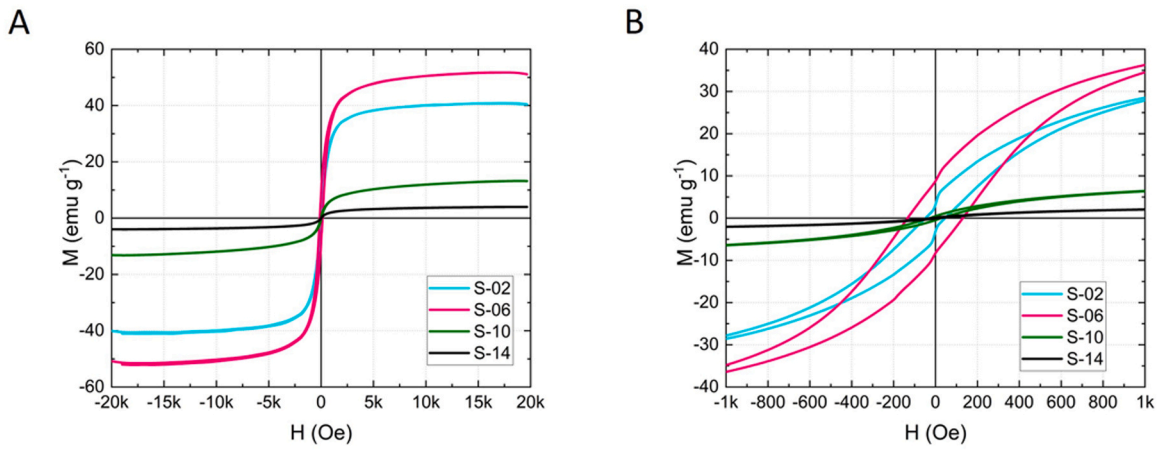

Fig. 10. Magnetization curves M vs. H of S-02 (cyan), S-06 (pink), S-10 (olive), and S-14 (black) samples. Panel A) refers to the full scale, whereas Panel B) shows the magnetization curve enlargement to highlight the middle section of the hysteresis loop.

Table 2
Magnetic properties of four selected samples (*i.e.*, S-02, S-06, S-10, and S-14) measured at RT.

Sample name	M_s (emu g^{-1})	M_r (emu g^{-1})	H_c (Oe)
S−02	40.76	3.15	46.50
S−06	51.76	8.51	132.00
S−10	13.21	0.46	27.25
S−14	3.98	1.00	17.55

hydroxide ions, and to self-assemble into one-dimensional chain-like structures once in water environment [22], thus favoring the growth of linear nanostructures [23]. Furthermore, PEG molecules inhibit also the agglomeration phenomena between the growing nuclei, and tend to adsorb at the surface of formed nuclei with different adsorption strength depending on the different crystal faces, thus causing the faster growth of nanocrystals in the direction with weaker surfactant adsorption.

Moreover, magnetite is characterized by an inverse spinel face-centered cubic (fcc) structure sublattice [42], and NPs shape is determined by the ratio between the growth rate along specific crystal plane directions, with nanorods preferentially formed when the growth rate is higher along the [110] direction [43,44]. This process is kinetically favored by the adsorption of PEG molecules on magnetite crystal planes, which can restrict the direction of the growing crystals [45]. This aspect is specifically true for samples obtained in water/PEG400, whereas the behavior of samples obtained in 2-pr./PEG400 can be correlated to the effects induced by both the complexation ability of the solvents, and the boiling points of the medium.

In fact, at the selected experimental conditions (*i.e.*, 150°C in hydrothermal reactor), a higher internal autogenous pressure is expected in a 2-pr.-rich confined environment with respect to a water-rich one [8]. This is easily rationalized based on the slightly lower boiling point of 2-propanol (82.6°C) with respect to water, enabling an earlier boiling and achievement of higher autogenous pressure in the hydrothermal reactor. Higher pressures are related to higher dielectric constant, likely affecting the growth mechanism. According to Demazeau [46], the stabilization of a specific structural form is induced by the kinetics of the solvothermal reaction, with a predominant role played by the intermediate metal complexes which can either speed up or slow down the kinetics, leading to either a metastable (or the thermodynamically stable) form. This is for instance the case of the solvothermal synthesis of MnS with different structural forms depending on the solvents selected, with formation of the thermodynamically stable α-form (spherical) in the synthesis carried out in presence of either water or ethylenediamine (*i.e.*, solvents able to stabilize the formation of the Mn complexes), and formation of metastable β- and γ-forms (rod and branched structures) if the synthesis is carried out in presence of tetrahydrofuran and benzene (*i.e.*, solvents unable to induce the complexation of Mn^{2+}) [47].

Regarding the role played by the autogenous pressure, Demazeau [46] reported that pressure can play different roles, namely: (i) the stabilization of more dense structures, if the pressure range is large enough, (ii) the enlargement of the thermal stability domain of the reactants, and (iii) the enhancement of the chemical reactivity, and of the kinetics of the involved reactions.

However, it should be considered also the manifold role played by the solvent as dispersion medium, and its physico-chemical properties, which might strongly influence the solubility and transport behavior of the precursors, also influencing the nucleation and growth of the NPs [48].

Lastly, since magnetite is a mixed ferrous-ferric oxide, increasing the content of the reducing sodium thiosulfate induced a better control over the oxidation state of iron, preserving the system from the complete oxidation and favoring the formation of magnetite rather than hematite, which is the thermodynamically most stable phase. The explanation of this specific behavior is the ability of thiosulfate ion (a soft base) to coordinate ferrous ion (a soft acid) in the presence of an alkaline environment, thus forming the possible complex $[Fe(S_2O_3)_2(OH)_2]^{4-}$ [21, 45]. As reported by Lian *et al.* [45], the competition between thiosulfate and the hydroxyl ions from the alkaline medium in presence of PEG molecules may play a key role in the assembly and growth of magnetite anisotropic NPs.

By analyzing the available literature, it should be pointed out that, since this is the first time that a mixed water/2-propanol/PEG400 hydrosolvothermal approach has been used to directly synthesize iron oxide NPs, it is difficult to find a suitable case study for a direct (and useful) comparison. However, to the best of the present authors knowledge, two studies can provide useful information.

The first one is the study by Harraz [21], which it has been also used as starting point for the actual experimental design object of the present study. In this study, the author investigated the production of magnetite nanowires in a water/PEG4000 environment (thus in absence of 2-propanol, and exploiting PEG4000 rather than PEG400), using sodium thiosulfate as reducing agent and NaOH as precipitating agent. Results reported that pure-phase magnetite nanowires *ca.* 1.5 μm length with average diameter of *ca.* 25 nm were obtained. Furthermore, the author found also that, at low PEG content, the co-presence of magnetite and hematite phases was pointed out. This result confirmed that it is possible to exert a control over the phase formation within the iron oxide nanostructures by varying the water/PEG volume ratios. By making a comparison with our study, it clearly emerged that probably the use of a low molecular weight PEG (*i.e.,* PEG400 rather than PEG4000) is probably one of the reasons why traces of hematite were evidenced in

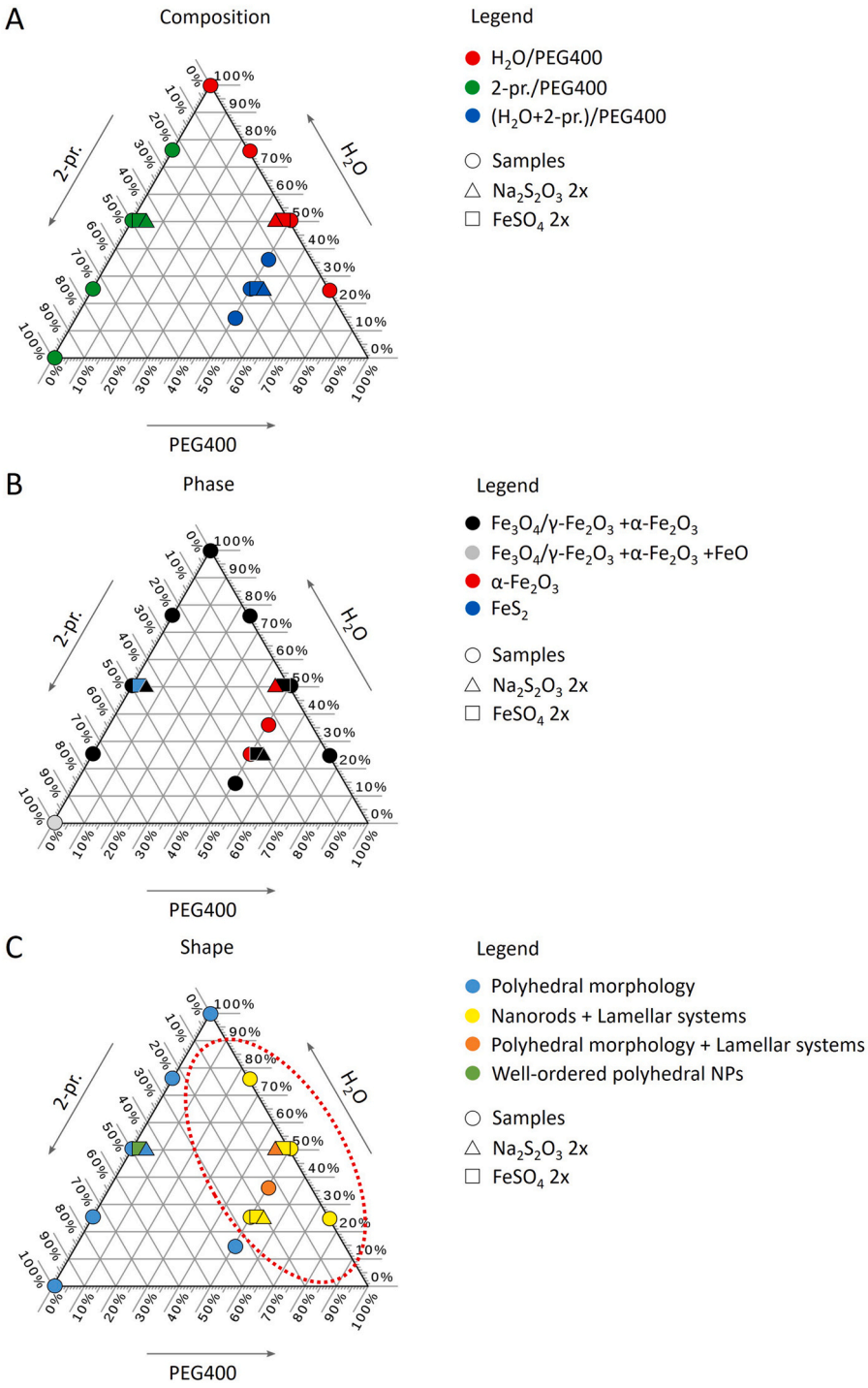

Fig. 11. Ternary diagrams reporting the chemical composition (expressed as volume % ratio) of the reaction medium (A), different phases (B), and the different shapes (C) of the NPs. Legend: ordinary samples (circles), samples obtained with double $Na_2S_2O_3{\cdot}5\ H_2O$ content (triangles), samples obtained with double $FeSO_4{\cdot}7\ H_2O$ (square). In panel (A), the color legend is the following: samples obtained from a water/PEG400 mixture (red), samples obtained from a 2-pr./PEG400 mixture (green), samples obtained from a (water/2-pr.)/PEG400 mixture (blue). In panel (B), the color legend is the following: samples showing a prevalence of $Fe_3O_4/\gamma\text{-}Fe_2O_3$ over $\alpha\text{-}Fe_2O_3$ phase (black), samples showing a prevalence of $Fe_3O_4/\gamma\text{-}Fe_2O_3$ over $\alpha\text{-}Fe_2O_3$ phase but containing also traces of FeO (grey), samples showing a prevalence of $\alpha\text{-}Fe_2O_3$ phase (red), samples showing a prevalence of pyrite (blue). In panel (C), the color legend is the following: samples showing a prevalence of polyhedral morphology (blue), samples showing a prevalence of nanorods and lamellar systems (yellow), samples showing a prevalence of polyhedral morphology and lamellar systems (orange), samples showing well-ordered polyhedral NPs (green).

the final products. However, apart from the crystal structure composition, the morphology of the samples obtained by Herraz [21] is very similar to the ones obtained in our study at analogous experimental conditions, even if in our case nanorods are shorter and thicker with co-presence of hematite lamellar systems (*i.e.*, samples S-02, S-03, and S-04).

The second relevant study is the one by Zhang et al. [19] where the use of a mixed water/ethylene glycol hydro-solvothermal route for the synthesis mesoporous magnetite NPs has been reported. In their study, authors reported that large non-porous polyhedral hematite NPs were

Table 3
Morphology, crystal phase, and magnetic response of samples.

Sample	Morphology	Crystal phase	Magnetic response
S−01	Polyhedral morphology	Fe_3O_4/γ-Fe_2O_3 + α-Fe_2O_3	Yes
S−02	Nanorods + Lamellar systems	Fe_3O_4/γ-Fe_2O_3 + α-Fe_2O_3	Yes
S−03	Nanorods + Lamellar systems	Fe_3O_4/γ-Fe_2O_3 + α-Fe_2O_3	Yes
S−04	Nanorods + Lamellar systems	Fe_3O_4/γ-Fe_2O_3 + α-Fe_2O_3	Yes
S−05	Polyhedral morphology	Fe_3O_4/γ-Fe_2O_3 + α-Fe_2O_3 + FeO	Yes
S−06	Polyhedral morphology	Fe_3O_4/γ-Fe_2O_3 + α-Fe_2O_3	Yes
S−07	Polyhedral morphology	Fe_3O_4/γ-Fe_2O_3 + α-Fe_2O_3	Yes
S−08	Polyhedral morphology	Fe_3O_4/γ-Fe_2O_3 + α-Fe_2O_3	Yes
S−09	Polyhedral morphology + Lamellar systems	α-Fe_2O_3	No
S−10	Nanorods + Lamellar systems	α-Fe_2O_3	No
S−11	Polyhedral morphology	Fe_3O_4/γ-Fe_2O_3 + α-Fe_2O_3	Yes
S−12	Polyhedral morphology + Lamellar systems	α-Fe_2O_3	No
S−13	Polyhedral morphology	Fe_3O_4/γ-Fe_2O_3 + α-Fe_2O_3	Yes
S−14	Nanorods + Lamellar systems	Fe_3O_4/γ-Fe_2O_3 + α-Fe_2O_3	Yes
S−15	Nanorods + Lamellar systems	Fe_3O_4/γ-Fe_2O_3 + α-Fe_2O_3	Yes
S−16	Well-ordered polyhedral NPs	FeS_2	No
S−17	Nanorods + Lamellar systems	Fe_3O_4/γ-Fe_2O_3 + α-Fe_2O_3	Yes

obtained in pure water environment, whereas large non-porous spherical magnetite NPs were obtained in pure ethylene glycol environment. Interestingly, mixed water/ethylene glycol environment allows obtaining a gradual reduction of the NPs average size by gradually increasing the water content with formation of mesopores. These results confirmed the double role played by the two solvents, with water acting as binder able to coordinate ferric ions and carrier of the precipitating agents, and ethylene glycol acting also as reducing agent. Analogous considerations can be translated to our system, with PEG400 playing a key role for its ability in forming a stable complex with Fe ions and as structure directing agent.

4. Conclusions

A novel alternative mixed hydro-solvothermal route has been investigated for the synthesis of anisotropic magnetic iron oxide NPs. The syntheses were performed at mild conditions (150 °C), selecting water, 2-propanol, or a mixture of them as reaction medium, in presence of PEG400 as structure directing agent, sodium thiosulfate as reducing agent, and NaOH as precipitating agent. Experimental results clearly demonstrate that at the experimental conditions selected it was not possible to obtain a pure magnetite/maghemite phase, but there was always co-presence of traces of hematite phase. In particular, in the case of the ternary water/2-propanol/PEG400 environment, it has been registered a predominance of hematite phase over the other phases. As expected, the increment of the reducing agent sodium thiosulfate concentration seems favoring the formation of magnetite/maghemite phase with respect to the hematite phase.

Concerning the particles morphology, nanorod particles were obtained only in water/PEG400 environment, whereas 2-propanol/PEG400 environment favors the growth of polyhedral systems. In all cases, the formation of nanorods was accompanied by the co-presence of lamellar systems. In the case of the synthesis in a mixed ternary water/2-propanol/PEG400 environment with equal amount of water/2-propanol, the produced nanorods result being thicker than their analogous obtained in a water/PEG400 environment (*i.e.*, in absence of 2-pr.).

The magnetic characterization highlighted that samples obtained from both bare water/PEG400 and 2-propanol/PEG400 environments (*i.e.*, with high content of magnetite/maghemite phase) possess high magnetic saturation values, whereas samples obtained from a mixed ternary water/2-propanol/PEG400 environment (*i.e.*, characterized by a predominance of hematite phase) show a remarkably lower magnetic saturation value.

In summary, the present study clearly indicates that the synthetic route here proposed is a promising approach for the synthesis of iron oxide systems with a prevalent anisotropic morphology at relatively mild conditions. At present, the main limitation of this protocol is the difficulty in obtaining pure magnetite/maghemite systems, being this targeted composition always affected by the co-presence of traces of hematite phase, with only few experimental conditions where pure hematite phase has been obtained. Surely an optimization of the process conditions is mandatory to drive the reaction toward the production of pure magnetite/maghemite systems (maybe varying the ratios and/or the nature of the reducing agents, or carefully tuning the molecular weight of the PEG used as in [21]).

Furthermore, these preliminary, though encouraging, results need a deeper investigation aiming at unveiling the role played by different organic solvents in controlling the final morphology and chemical structure, since mixtures of different organic solvents have different physicochemical properties and polarity.

Regarding the possible implications and perspective applications of the results of this study, it should be considered that the possibility of synthesizing anisotropic magnetite NPs at relatively mild conditions following a mixed hydro-solvothermal route can be an interesting alternative process potentially exploitable in many technological fields where the use of magnetic particles with controlled size and shape can play a key role (*e.g.*, photo-induced environmental remediation processes [49], biomedical/clinical uses and magnetic hyperthermia [50], drug-delivery [51], sensing and imaging [52], electronics [53], and many others).

CRediT authorship contribution statement

Gabriele Bona: Writing – review & editing, Investigation, Formal analysis. **Giulia Bragaggia:** Writing – review & editing, Writing – original draft, Investigation, Formal analysis. **Barbara Di Credico:** Writing – review & editing, Investigation. **Silvia Mostoni:** Writing – review & editing, Investigation, Formal analysis. **Giancarlo Capitani:** Formal analysis, Investigation, Writing – review & editing. **Matteo Cantoni:** Writing – review & editing, Resources, Investigation, Formal analysis. **Roberto Nisticò:** Writing – review & editing, Writing – original draft, Supervision, Resources, Investigation, Formal analysis, Conceptualization. **Roberto Scotti:** Writing – review & editing, Writing – original draft, Supervision, Resources, Investigation. **Silvia Gross:** Writing – review & editing, Writing – original draft, Supervision, Resources, Investigation, Conceptualization.

Declaration of Competing Interest

The authors declare that they have no known competing financial interests or personal relationships that could have appeared to influence the work reported in this paper

Data availability

Data will be made available on request.

Acknowledgements

This work received financial support from MUR (Italy) through both PRIN Project MAPEC (N. 2022599NR3), and PRIN Project PERFECT (N. P2022TK9B9), which are gratefully acknowledged. University of Milano-Bicocca is gratefully acknowledged for funding project Premio Giovani Talenti 2022. R.N. would like to acknowledge Dr. Paolo Gentile and Dr. Fabrizio Vergani (University of Milano-Bicocca, Italy) for the technical support during the SEM analysis, and Dr. Melissa Saibene (University of Milano-Bicocca, Italy) for the TEM-SAED analysis. The magnetic characterization was performed at Polifab, the micro and nanofabrication facility of Politecnico di Milano (Italy).

Appendix A. Supporting information

Supplementary data associated with this article can be found in the online version at doi:10.1016/j.colsurfa.2024.135117.

References

[1] P. Azcona, R. Zysler, V. Lassalle, Simple and novel strategies to achieve shape and size control of magnetite nanoparticles intended for biomedical applications, Colloid Surf. A Physicochem. Eng. Asp. 504 (2016) 320–330, https://doi.org/10.1016/j.colsurfa.2016.05.064.
[2] R. Nisticò, A synthetic guide toward the tailored production of magnetic iron oxide nanoparticles, Bol. Soc. Esp. Ceram. V. 60 (2021) 29–40, https://doi.org/10.1016/j.bsecv.2020.01.011.
[3] R. Nisticò, F. Cesano, F. Garello, Magnetic materials and systems: Domain structure visualization and other characterization techniques for the application in the materials science and biomedicine, Inorganics 8 (2020) 6, https://doi.org/10.3390/inorganics8010006.
[4] S. Polarz, Shape matters: anisotropy of the morphology of inorganic colloidal particles – synthesis and function, Adv. Funct. Mater. 21 (2011) 3214–3230, https://doi.org/10.1002/adfm.201101205.
[5] A.-G. Niculescu, C. Chircov, A.M. Grumezescu, Magnetite nanoparticles: synthesis methods – a comparative review, Methods 199 (2022) 16–27, https://doi.org/10.1016/j.ymeth.2021.04.018.
[6] A. Arakari, F. Masuda, Y. Amemiya, T. Tanaka, T. Matsunaga, Control of the morphology and size of magnetite particles with peptides mimicking the Mms6 protein from magnetotactic bacteria, J. Colloid Interface Sci. 343 (2010) 65–70, https://doi.org/10.1016/j.jcis.2009.11.043.
[7] C. Sanchez, L. Rozes, F. Ribot, C. Laberty-Robert, D. Grosso, C. Sassoye, C. Boissiere, L. Nicole, "Chimie douce": a land of opportunities for the designed construction of functional inorganic and hybrid organic-inorganic nanomaterials, C. R. Chim. 13 (2010) 3–39, https://doi.org/10.1016/j.crci.2009.06.001.
[8] S. Diodati, R.I. Walton, S. Mascotto, S. Gross, Low-temperature wet chemistry synthetic approaches towards ferrites, Inorg. Chem. Front. 7 (2020) 3282–3314, https://doi.org/10.1039/D0QI00294A.
[9] S. Feng, R. Xu, New materials in hydrothermal synthesis, Acc. Chem. Res. 34 (2001) 239–247, https://doi.org/10.1021/ar0000105.
[10] J.-Q. Wang, Y.-X. Huang, Y. Pan, J.-X. Mi, Hydrothermal synthesis of high purity zeolite A from natural kaolin without calcination, Microporous Mesoporous Mater. 199 (2014) 50–56, https://doi.org/10.1016/j.micromeso.2014.08.002.
[11] G. Demazeau, Solvothermal and hydrothermal processes: the main physico-chemical factors involved and new trends, Res. Chem. Intermed. 37 (2011) 107–123, https://doi.org/10.1007/s11164-011-0240-z.
[12] R. Srivastava, K.N. Khanna, Stokes−Einstein relation in two- and three-dimensional fluids, J. Chem. Eng. Data 54 (2009) 1452–1456, https://doi.org/10.1021/je800698t.
[13] B. Derjaguin, L. Landau, Theory of the stability of strongly charged lyophobic sols and of the adhesion of strongly charged particles in solutions of electrolytes, Acta Physicochim. URSS 14 (1941) 633–662.
[14] E.J.W. Verwey, Theory of the stability of lyophobic colloids, J. Phys. Chem. 51 (1947) 631–636, https://doi.org/10.1021/j150453a001.
[15] Y. He, Y. Zhu, N. Wu, Mixed solvents: a key in solvothermal synthesis of $KTaO_3$, J. Solid State Chem. 177 (2004) 2985–2990, https://doi.org/10.1016/j.jssc.2004.04.051.
[16] A. Nohara, S. Takeshita, T. Isobe, Mixed-solvent strategy for solvothermal synthesis of well-dispersed YBO_3:Ce^{3+},Tb^{3+} nanocrystals, RSC Adv. 4 (2014) 11219–11224, https://doi.org/10.1039/C3RA47864E.
[17] E. Miniach, G. Gryglewicz, Solvent-controlled morphology of bismuth sulfide for supercapacitor applications, J. Mater. Sci. 53 (2018) 16511–16523, https://doi.org/10.1007/s10853-018-2785-3.
[18] B.-S. Wu, P. Wang, J. Song, Mixed-solvothermal synthesis and morphology-dependent electrochemical properties of α-Fe_2O_3 nanoparticles for lithium-ion batteries, J. Mater. Sci.: Mater. Electron. 31 (2020) 6779–6785, https://doi.org/10.1007/s10854-020-03236-7.
[19] Y. Zhang, C. Li, L. Liu, K. Wang, Y. Zhu, J. Ben, J. Wu, Solvothermal synthesis of mesoporous Fe_3O_4 nanoparticles in mixed solvent of ethylene glycol and water: structure and magnetic properties, J. Supercond. Nov. Magn. 32 (2019) 757–762, https://doi.org/10.1007/s10948-018-4766-9.
[20] T. Xin, M. Ma, H. Zhang, J. Gu, S. Wang, M. Liu, Q. Zhang, A facile approach for the synthesis of magnetic separable Fe_3O_4@TiO_2, core–shell nanocomposites as highly recyclable photocatalysts, Appl. Surf. Sci. 288 (2014) 51–59, https://doi.org/10.1016/j.apsusc.2013.09.108.
[21] F.A. Harraz, Polyethylene glicol-assisted hydrothermal growth of magnetite nanowires: synthesis and magnetic properties. Phys. E 40 (2008) 3131–3136, https://doi.org/10.1016/j.physe.2008.05.007.
[22] S. Chen, J. Feng, X. Guo, J. Hong, W. Ding, One-step wet chemistry for preparation of magnetite nanorods, Mater. Lett. 59 (2005) 985–988, https://doi.org/10.1016/j.matlet.2004.11.043.
[23] J. Wang, Z. Peng, Y. Huang, Q. Chen, Growth of magnetite nanorods along its easy-magnetization axis of [1 1 0], J. Cryst. Growth 263 (2004) 616–619, https://doi.org/10.1016/j.jcrysgro.2003.11.102.
[24] F. Cesano, G. Fenoglio, L. Carlos, R. Nisticò, One-step synthesis of magnetic chitosan polymer composite films, Appl. Surf. Sci. 345 (2015) 175–181, https://doi.org/10.1016/j.apsusc.2015.03.154.
[25] S.P. Schwaminger, D. Bauer, P. Fraga-Garcia, F.E. Wagner, S. Berensmeier, Oxidation of magnetite nanoparticles: impact on surface and crystal properties, CrystEngComm 19 (2017) 246–255, https://doi.org/10.1039/C6CE02421A.
[26] Y. Shen, Q. Zhao, X. Li, Y. Hou, Comparative investigation of visible-light-induced benzene degradation on M-ferrite/hematite (M = Ca, Mg, Zn) nanospheres by in situ FTIR: Intermediates and reaction mechanism, Colloid Surf. A Physicochem. Eng. Asp. 618 (2021) 126501, https://doi.org/10.1016/j.colsurfa.2021.126501.
[27] J. Zhai, J. Brugger, A. Pring, Mechanism and kinetics of hydrothermal replacement of magnetite by hematite, Geosci. Front. 10 (2019) 29–41, https://doi.org/10.1016/j.gsf.2018.05.015.
[28] Z. Li, C. Chaneac, G. Berger, S. Delaunay, A. Graff, G. Lefevre, Mechanism and kinetics of magnetite oxidation under hydrothermal conditions, RSC Adv. 9 (2019) 33633–33642, https://doi.org/10.1039/C9RA03234G.
[29] C.-J. Chen, R.-K. Chiang, H.-Y. Lai, C.-R. Lin, Characterization of monodisperse wüstite nanoparticles following partial oxidation, J. Phys. Chem. C. 114 (2010) 4258–4263, https://doi.org/10.1021/jp908153y.
[30] M. Yin, Z. Chen, B. Deegan, S. O'Brien, Wüstite nanocrystals: synthesis, structure and superlattice formation, J. Mater. Res. 22 (2007) 1987–1995, https://doi.org/10.1557/jmr.2007.0247.
[31] M. Hamada, S. Ganschow, D. Klimm, G. Serghiou, H.-J. Reichmann, M. Bickermann, Wüstite ($Fe_{1-x}O$) – thermodynamics and crystal growth, Z. Naturforsch. B 77 (2022) 463–468, https://doi.org/10.1515/znb-2022-0071.
[32] J.M. Meijer, L. Rossi, Preparation, properties, and applications of magnetic hematite microparticles, Soft Matter 17 (2021) 2354–2368, https://doi.org/10.1039/D0SM01977A.
[33] H. Qin, J. Jia, L. Lin, H. Ni, M. Wang, L. Meng, Pyrite FeS_2 nanostructures: synthesis, properties and applications, Mater. Sci. Eng. B 236-237 (2018) 104–124, https://doi.org/10.1016/j.mseb.2018.11.003.
[34] M.A. Khan, J.C. Sarker, S. Lee, S.C. Mangham, M.O. Manareh, Synthesis, characterization and processing of cubic iron pyrite nanocrystals in a photovoltaic cell, *Mater. Chem. Phys.* 148 (2014) 1022–1028, https://doi.org/10.1016/j.matchemphys.2014.09.013.
[35] N. E'jazi, M. Aghaziarati, Determination of optimum condition to produce nanocrystalline pyrite by solvothermal synthesis method, Adv. Powder Technol. 23 (2012) 352–357, https://doi.org/10.1016/j.apt.2011.04.010.
[36] H. Gavilan, K. Simeonidis, E. Myrovali, E. Mazario, O. Chubykalo-Fesenko, R. Chantrell, Ll Balcells, M. Angelakeris, M.P. Morales, D. Serantes, How size, shape and assembly of magnetic nanoparticles give rise to different hyperthermia scenarios, Nanoscale 13 (2021) 15631–15646, https://doi.org/10.1039/D1NR03484G.
[37] Y. Hadadian, H. Masoomi, A. Dinari, C. Ryu, S. Hwang, S. Kim, B.K. Cho, J.Y. Lee, J. Yoon, From low to high saturation magnetization in magnetite nanoparticles: the crucial role of the molar ratios between the chemicals, ACS Omega 7 (2022) 15996–16012, https://doi.org/10.1021/acsomega.2c01136.
[38] S. Sun, H. Zeng, D.B. Robinson, S. Raoux, P.M. Rice, S.X. Wang, G. Li, Monodisperse MFe_2O_4 (M = Fe, Co, Mn) nanoparticles, J. Am. Chem. Soc. 126 (2004) 273–279, https://doi.org/10.1021/ja0380852.
[39] A.-H. Lu, E.L. Salabas, F. Schuth, Magnetic nanoparticles: synthesis, protection, functionalization, and application, Angew. Chem. Int. Ed. 46 (2007) 1222–1244, https://doi.org/10.1002/anie.200602866.
[40] S.A. Rajan, M. Sharma, N.K. Sahu, Water-to-PEG variation: morphology and hyperthermic behaviour of iron oxide, J. Supercond. Nov. Magn. 33 (2020) 1603–1609, https://doi.org/10.1007/s10948-019-05155-z.
[41] C. Li, R. Wei, Y. Xu, A. Sun, L. Wei, Synthesis of hexagonal and triangular Fe_3O_4 nanosheets via seed-mediated solvothermal growth, Nano Res 7 (2014) 536–543, https://doi.org/10.1007/s12274-014-0421-3.
[42] S. Baghshahi, F. Yousefi, A new systematic approach to the morphology and magnetic properties of spherical, cubic, and rod-like magnetite nanoparticles, J. Supercond. Nov. Magn. 34 (2021) 1949–1954, https://doi.org/10.1007/s10948-021-05884-0.
[43] Z.L. Wang, Transmission electron microscopy of shape-controlled nanocrystals and their assemblies, J. Phys. Chem. B 104 (2000) 1153–1175, https://doi.org/10.1021/jp993593c.
[44] R. Nisticò, P. Rivolo, F. Giorgis, Tips and tricks for the surface engineering of well-ordered morphologically driven silver-based nanomaterials, ChemistryOpen 8 (2019) 508–519, https://doi.org/10.1002/open.201900007.

[45] S. Lian, Z. Kang, E. Wang, M. Jiang, C. Hu, L. Xu, Convenient synthesis of single crystalline magnetic Fe_3O_4 nanorods, Solid State Commun. 127 (2003) 605–608, https://doi.org/10.1016/S0038-1098(03)00580-5.
[46] G. Demazeau, Solvothermal processes: definition, key factors governing the involved chemical reactions and new trends, Z. Naturforsch. B 65 (2010) 999–1006, https://doi.org/10.1515/znb-2010-0805.
[47] J. Mu, Z. Gu, L. Wang, Z. Zhang, H. Sun, S.-Z. Kang, Phase and shape controlling of MnS nanocrystals in the solvothermal process, J. Nanopart. Res. 10 (2008) 197–201, https://doi.org/10.1007/s11051-007-9216-8.
[48] J. Yang, J.-h Zeng, S.H. Yu, L. Yang, Y.-H. Zhang, Y.-T. Qian, Pressure-controlled fabrication of stibnite nanorods by the solvothermal decomposition of a simple single-source precursor, Chem. Mater. 12 (2000) 2924–2929, https://doi.org/10.1021/cm000031t.
[49] J. Shi, J. Zhang, C. Wang, Y. Liu, J. Li, Research progress on the magnetite nanoparticles in the fields of water pollution control and detection, Chemosphere 336 (2023) 139220, https://doi.org/10.1016/j.chemosphere.2023.139220.
[50] Y. Pineiro, Z. Vargas, J. Rivas, M.A. Lopez-Quintela, Iron oxide based nanoparticles for magnetic hyperthermia strategies in biological applications, Eur. J. Inorg. Chem. 2015 (2015) 4495–4509, https://doi.org/10.1002/ejic.201500598.
[51] F. Parsa, M. Setoodehkhah, S.M. Atyabi, Loading and release study of ciprofloxacin from silica-coated magnetite modified by iron-based metal-organic framework (MOF) as a nonocarrier in targeted drug delivery system, Inorg. Chem. Commun. 155 (2023) 111056, https://doi.org/10.1016/j.inoche.2023.111056.
[52] A. Mohsin, M.H. Hussain, M.Z. Mohsin, W.Q. Zaman, M.S. Aslam, A. Shan, Y. Dai, I. M. Khan, S. Niazi, Y. Zhuang, M. Guo, Recent advances of magnetic nanomaterials for bioimaging, drug delivery, and cell therapy, ACS Appl. Nano Mater. 5 (2022) 10118–10136, https://doi.org/10.1021/acsanm.2c02014.
[53] S. Alipour, A. Pourjavadi, S.H. Hosseini, Magnetite embedded κ-carrageenan-based double network nanocomposite hydrogel with two-way shape memory properties for flexible electronics and magnetic actuators, Carbohydr. Polym. 310 (2023) 120610, https://doi.org/10.1016/j.carbpol.2023.120610.